Molecular Architecture *via* Coordination: Self-Assembly, Characterization, and Host−Guest Chemistry of Mixed, Neutral-Charged, Pt−Pt and Pt−Pd Macrocyclic Tetranuclear Complexes. X-ray Crystal Structure of Cyclobis[[*cis*-Pt(dppp)(4-ethynylpyridine)$_2$][*cis*-Pd^{2+}(PEt$_3$)$_2$2$^-$OSO$_2$CF$_3$]]

Jeffery A. Whiteford, Cuong V. Lu, and Peter J. Stang*

Contribution from the Department of Chemistry, The University of Utah, Salt Lake City, Utah 84112

Received October 8, 1996[⊗]

Abstract: Interaction of *cis*-Ptdppp(*p*-C$_6$H$_4$CN)$_2$ or *cis*-Ptdppp(*p*-C$_2$C$_6$H$_4$N)$_2$ with *cis*-ML$_2$(OSO$_2$CF$_3$)$_2$ (M = Pt or Pd; L = PEt$_3$ or L$_2$ = dppp), in CH$_2$Cl$_2$ or acetone, at room temperature, results in mixed, neutral-charged cyclic tetranuclear, Pt−Pt or Pt−Pd macrocyclic complexes in 90−99% yields *via* self-assembly. All tetramers are microcrystalline air- and water-stable solids with decomposition points > 170 °C. The benzonitrile based macrocycles can be disassembled in solution with 4,4′-bipyridine, while the 4-ethynylpyridine systems are more stable toward a variety of guests. The 4-ethynylpyridine tetramers display host−guest chemistry with silver triflate *via* the "π -tweezer effect". The X-ray crystal structure as well as FABMS, including isotope patterns, are reported for the tetranuclear macrocycle cyclobis[[*cis*-Pt(dppp)(4-ethynylpyridine)$_2$][*cis*-Pd^{2+}(PEt$_3$)$_2$2$^-$OSO$_2$CF$_3$]] (**14**).

Introduction

Self-assembly is the most efficient means for the synthesis of a variety of discrete supramolecular species.[1−3] Recently transition metal directed self-assembly *via* coordination has emerged as a new and major motif in supramolecular architecture.[4,5] This motif offers a variety of design features, such as (a) tremendous versatility due to the potentially large and diverse number of suitable transition metal complexes and multidentate ligands available as building blocks; (b) bond energies in between the range of the strong covalent bonding in classical macrocycles and the weak interactions (hydrogen bonding, $\pi-\pi$-stacking, hydrophobic and hydrophilic forces, electrostatic interactions, etc.) of systems patterned after biological models;[4,6] (c) excellent product yields, due to self-assembly; (d) ready adaptability to diverse supramolecular species including 3-D structures; (e) enormous design variations by virtue of the permutation of linkers and corners; (f) etc.

To date, chelation and coordination have primarily been employed in the formation of hitherto unknown molecular squares,[5,7] with unique, well defined shapes and geometries. However, currently only all cationic,[5,7] anionic,[8c] or neutral[8a,b,d] molecular squares are known. Likewise, only homonuclear or hybrid transition metal-iodonium molecular squares have been prepared with no examples of heteronuclear tetramers. One of

[⊗] Abstract published in *Advance ACS Abstracts,* March 1, 1997.

(1) Recent reviews: (a) Philip, D.; Stoddart, J. F. *Angew. Chem., Int. Ed. Engl.* **1996**, *35*, 1154−1196. (b) Tour, J. M. *Chem. Rev.* **1996**, *96*, 537−553. (c) Lehn, J.-M. *Supramolecular Chemistry: Concepts and Perspectives*; VCH Publishers: Weinheim, 1995. (d) Amabilino, D. B.; Stoddart, J. F. *Chem. Rev.* **1995**, *95*, 2725−2828. (e) Lawrence, D. S.; Jiang, T.; Levett, M. *Chem. Rev.* **1995**, *95*, 2229−2260. (f) Philp, D.; Stoddart, J. F. *Angew. Chem., Int. Ed. Engl.* **1995**, *35*, 1154−1196. (g) Whitesides, G. M.; Simanek, E. E.; Mathias, J. P.; Seto, C. T.; Chin, D. N.; Mammen, M.; Gordon, D. M. *Acc. Chem. Res.* **1995**, *28*, 37−44. (h) Cram, D. J.; Cram, J. M. *Container Molecules and Their Guests*; The Royal Society of Chemistry: Cambridge, England, 1994. (i) Ball, P. *Designing the Molecular World*; Princeton University Press: Princeton, NJ, 1994.

(2) (a) *Monographs in Supramolecular Chemistry 1−5*; Stoddart, J. F., Ed.; Royal Society of Chemistry: Cambridge, 1989; 1991; and 1994−1995. (b) *Supramolecular Chemistry*; Balzzani, V., DeCola, L., Eds.; Kluwer Academic Publishers: The Netherlands, 1992. (c) *Inclusion Phenomena and Molecular Recognition*; Atwood, J. L., Ed.; Plenum: New York, 1990. (d) *Molecular Inclusion and Molecular Recognition-Clathrates II (Topics in Current Chemistry, Vol. 149)*; Weber, E., Ed.; Springer-Verlag: New York, 1987. (e) *Host−Guest Complex Chemistry/Macrocycles*; Vogtle, F., Weber, E., Eds.; Springer-Verlag: Berlin, 1985.

(3) Drexler, K. E. *Nanosystems: Molecular Machinery, Manufacturing, and Computation*; Wiley; New York, 1992.

(4) Recent key references: (a) Amabilino, D. B.; Dietrich-Buchecker, C. O.; Sauvage, J.-P. *J. Am. Chem. Soc.* **1996**, *118*, 3285−3286. (b) Fujita, M.; Oguro, D.; Miyazawa, M.; Oka, H.; Yamaguchi, K.; Ogura, K. *Nature* **1995**, *378*, 469−471. (c) Ashton, P. R.; Ballardini, R.; Balzani, V.; Credi, A.; Gandolfi, M. T.; Menzer, S.; Pérez-García, L.; Prodi, L.; Stoddart, J. F.; Venturi, M.; White, A. J. P.; Williams, D. J. *J. Am. Chem. Soc.* **1995**, *117*, 11171−11197. (d) Bedard, T. C.; Moore, J. S. *J. Am. Chem. Soc.* **1995**, *117*, 10662−10671. (e) van Nostrum, C. F.; Picken, S. J.; Schouten, A.-J.; Nolte, R. J. M. *J. Am. Chem. Soc.* **1995**, *117*, 9957−9965. (f) Chi, X.; Guerin, A. J.; Haycock, R. A.; Hunter, C. A.; Sarson, L. D. *J. Chem. Soc., Chem. Commun.* **1995**, 2563−2565. (g) Drain, C. M.; Lehn, J.-M. *J. Chem. Soc. Chem. Commun.* **1994**, 2313−2315.

(5) (a) Manna, J.; Whiteford, J. A.; Stang, P. J. *J. Am. Chem. Soc.* **1996**, *118*, 8731−8732. (b) Stang, P. J.; Whiteford, J. A. *Res. Chem. Intermed.* **1996**, *22*, 659−665. (c) Olenyuk, B.; Whiteford, J. A.; Stang, P. J. *J. Am. Chem. Soc.* **1996**, *118*, *35*, 8221−8230. (d) Stang, P. J.; Olenyuk, B. *Angew. Chem., Int. Ed. Engl.* **1996**, *35*, 732−736. (e) Stang, P. J.; Chen, K.; Arif, A. M. *J. Am. Chem. Soc.* **1995**, *117*, 8793−8797. (f) Stang, P. J.; Cao, D. H.; Saito, S.; Arif, A. M. *J. Am. Chem. Soc.* **1995**, *117*, 6273−6283. (g) Stang, P. J.; Chen, K. *J. Am. Chem. Soc.* **1995**, *117*, 1667−1668. (h) Stang, P. J.; Whiteford, J. A. *Organometallics* **1994**, *13*, 3776−3777. (i) Stang, P. J.; Cao, D. H. *J. Am. Chem. Soc.* **1994**, *116*, 4981−4982. (j) Stang, P. J.; Zhdankin, V. V. *J. Am. Chem. Soc.* **1993**, *115*, 9808−9809.

(6) (a) Schneider, H- *Angew. Chem., Int. Ed. Engl.* **1991**, *30*, 1417−1436. (b) Anelli, P. L.; Ashton, P. R.; Spencer, N.; Slawin, A. M. Z.; Stoddart, J. F.; Williams, D. J. *Angew. Chem., Int. Ed. Engl.* **1991**, *30*, 1036−1039.

(7) (a) Fujita, M.; Kwon, Y. J.; Washizu, S.; Ogura, K. *J. Am. Chem. Soc.* **1994**, *116*, 1151−1152. (b) Rauter, H.; Hillgeris, E. C.; Erxleben, A.; Lippert, B. *J. Am. Chem. Soc.* **1994**, *116*, 616−624. (c) Fujita, M.; Nagao, S.; Iida, M.; Ogata, K.; Ogura, K. *J. Am. Chem. Soc.* **1993**, *115*, 1574−1576. (d) Fujita, M.; Yazaki, J.; Ogura, K. *J. Am. Chem. Soc.* **1990**, *112*, 5645−5647.

(8) (a) Slone, R. V.; Hupp, J. T.; Stern, C. L.; Albrecht-Schmitt, T. E. *Inorg. Chem.* **1996**, *35*, 4096−4097. (b) Slone, R. V.; Yoon, D. I.; Calhoun, R. M.; Hupp, J. T. *J. Am. Chem. Soc.*, **1995**, *117*, 11813−11814. (c) Small, J. H.; McCord, D. J.; Greaves, J.; Shea, K. J. *J. Am. Chem. Soc.* **1995**, *117*, 11588−11589. (d) Stricklen, P. M.; Volcko, E. J.; Verkade, J. G. *J. Am. Chem. Soc.* **1983**, *105*, 2494−2495.

S0002-7863(96)03528-7 CCC: $14.00

Scheme 1

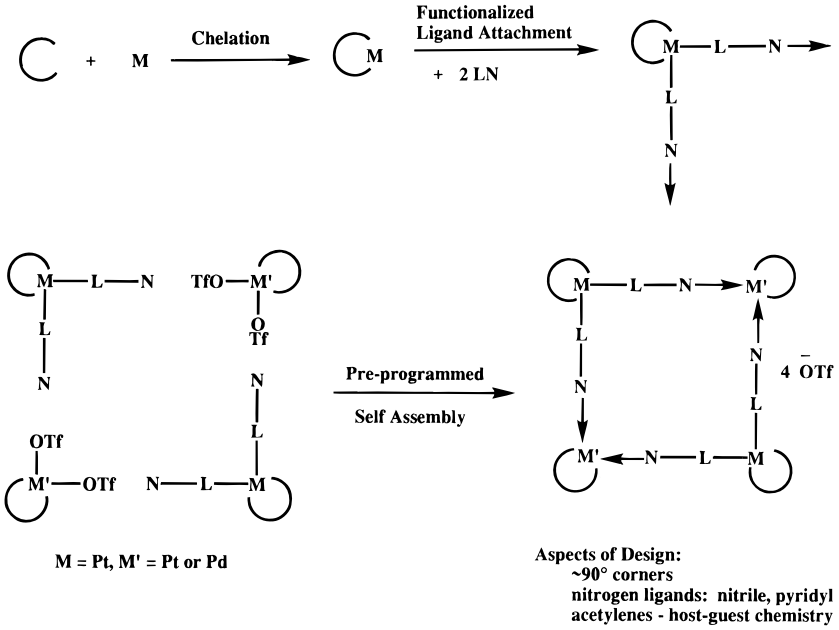

the major design advantages of coordination is the ability to vary the charge density (*via* different metals and/or different oxidation states) as well as the cavity size and shape (*via* the connector ligands) and thereby fine tune the potential host−guest and molecular recognition properties of the resultant supramolecular species.

In this paper we wish to report (1) the rational design and characterization of the first examples of mixed neutral-charged molecular squares; (2) the first examples of heteronuclear molecular squares; (3) the single crystal X-ray structure of a unique mixed neutral-charged heterobimetallic Pt−Pd molecular square; (4) incorporation of CC triple bonds (acetylenic units) as part of the connectors, and (5) studies on the host−guest properties, including π-coordination of Ag^+, *via* the π-tweezer effect, of these unique molecular squares.

Results and Discussion

The rational design of mixed neutral-charged and heterobimetallic molecular squares requires a modular self-assembly approach of appropriate subunits as complete self-assembly of the constituent parts would result in mixtures of products (*i.e.*, all neutral, all charged, mixed neutral-charged, homonuclear, heteronuclear, etc.). The simplest approach would involve use of the already available square planar Pt and Pd bistriflate complexes (**1**−**4**) for the charged portion in combination with "preconstructed" neutral monomeric units with built in connectors for the uncharged corners. This approach provides the added synergistic benefit of heteronuclear systems by simple variation of the metals in the two different subunits. The construction of the desired neutral connectors should be simple, preferably a single step process from readily available precursors (Scheme 1).

Indeed, the synthesis of neutral monomeric subunits **5** and **6** was easily accomplished using classical organic and organometallic techniques and commercially or well established easily available precursors. Lithium−halogen exchange of 4 equiv of 4-iodobenzonitrile at −78 °C with *n*-butyllithium in diethyl ether followed by immediate addition of 1 equiv of 1,3-bis(diphenylphosphino)propane (dppp) chelated Pt(II)Cl_2 gave, after workup, monomer **5** in 83% isolated yield (Scheme 2). Platinum monomer **6** was prepared similarly to monomer **5**. 4-Ethynylpyridine was synthesized by a modified Castro−Stevens coupling[9b] of 4-bromopyridine with trimethylsilylacetylene followed by treatment with TBAF in THF at 0 °C. Deprotonation of 2 equiv of 4-ethynylpyridine with *tert*-butyllithium at −78 °C in THF, followed by immediate addition of 1 equiv of 1,3-bis(diphenylphosphino)propane chelated Pt(II)Cl_2 afforded, after workup, the desired dppp chelated monomer **6**, in 68% isolated yield.

Reaction of **5** with an equimolar amount of **1** and **2**, respectively, in CH_2Cl_2 at room temperature results in the formation of neutral-charged tetranuclear complexes **7** and **8**, while reaction of **5** with **3** and **4**, respectively, in acetone at room temperature, resulted in the formation of neutral-charged tetranuclear complexes **9** and **10** (Scheme 2). In a similar fashion, reaction of **6** with an equimolar amount of **1** and **2**, respectively, in CH_2Cl_2 at room temperature, resulted in the formation of neutral-charged tetranuclear complexes **11** and **12**, while interaction of monomer **6** with **3** and **4**, respectively, in acetone at room temperature resulted in the formation of neutral-charged tetranuclear complexes **13** and **14** all in excellent isolated yields (Scheme 3). Although complexes **7**, **8**, **10**, **12**, and **14** form within a matter of minutes *via* self-assembly, complexes **9**, **11**, and **13** required 4 h for complete conversion to the respective tetranuclear macrocycles.

All eight tetranuclear complexes are stable microcrystalline solids with different coloration. Homonuclear complex **7** is light pink, whereas the homonuclear complexes **9**, **11**, and **13** are white. Heteronuclear complex **8** is reddish-brown, whereas the heteronuclear complexes **10**, **12**, and **14** are yellow. Mixed neutral-charged tetranuclear macrocycles **7**, **8**, **11**, and **12** are soluble in organic solvents such as CH_2Cl_2 and $CHCl_3$, while macrocycles **9**, **10**, **13**, and **14** are soluble in acetone and nitromethane.

These macrocyclic, tetranuclear triflate complexes have been fully characterized by analytical and spectral means as outlined in the Experimental Section. In particular, all new compounds have elemental analyses consistent with their respective compositions. The $^{31}P\{^1H\}$ spectra of **7**−**10** each show two singlets

(9) (a) Ciana, L.-D.; Haim, A. *J. Heterocycl. Chem.* **1984**, 607−608. (b) Takahashi, S.; Kuroyama, Y.; Sonogahira, K.; Hagihara, N. *Synthesis* **1980**, 627−630.

Scheme 2

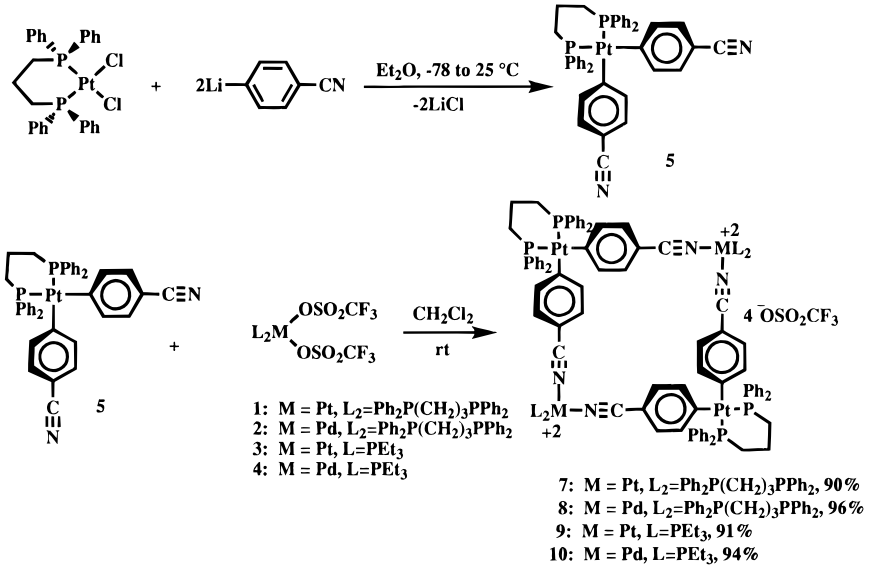

Scheme 3

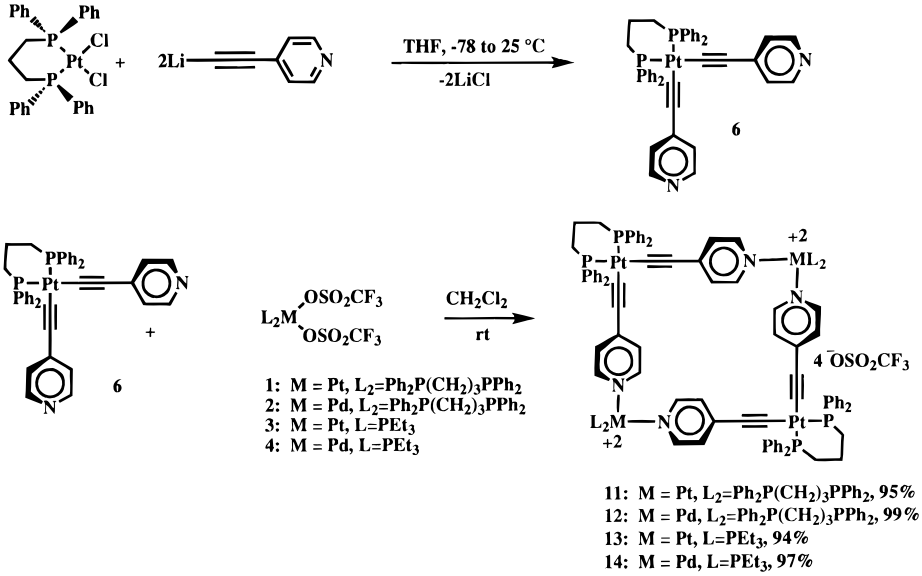

with a shift of 1.0−2.0 ppm for the P on the neutral Pt (P−Pt); 5.2 ppm for the P attached to the charged Pt (P−Pt^{2+}) for **7** and 4.8 ppm for the P−Pt^{2+} of **9**; 6.4 ppm for the P−Pd^{2+} of **8** and 4.8 ppm for the P−Pd^{2+} of **10**, respectively, relative to the precursors **1**−**5**. Diagnostic for the tetranuclear complexes **7**−**10** are the respective ^{1}H and ^{13}C{^{1}H} NMR spectra. The ^{1}H NMR signals for the methylenes of **7** and **8** for the charged metal chelating dppp units are shifted downfield, relative to the precursors **1**, **2**, and **5**, while the methylenes of the neutral metal chelating dppp units remain essentially unchanged. Also observed were overlapping aromatic resonances for the two sets of phenyl groups of the dppp ligand for **7** and **8**, while squares **9** and **10** have signals for the methyl and methylene groups of the triethylphosphine ligands. The two sets of aromatic resonances for the cyanobenzene unit (α and β to the CN) are virtually identical. Integration of the proton signals is in accord with the requirements for **7**−**10**. The ^{19}F spectra display singlets at −79 ppm for **7** and **8**, while **9** and **10** display singlets at −75 ppm, characteristic for ionic $CF_3SO_3^-$. The ^{31}P{^{1}H} spectra of **11**−**14** each show two singlets with a shift of 0.1−1.0 ppm for the P on the neutral Pt and 4.0 ppm for the P−Pt^{2+} of **11**; 9.3 ppm for the P−Pt^{2+} of **13**; 9.7 ppm for the P−Pd^{2+} of **12**; and 24.4 ppm for the P−Pd^{2+} of **14**, respectively, relative to the precursors **6** and **1**−**4**. Also diagnostic for the tetranuclear complexes **11**−**14** are the respective ^{1}H and ^{13}C{^{1}H} NMR spectra. Similar to **7** and **8**, the ^{1}H NMR signals for the methylenes of **11** and **12** for the charged metal chelating dppp units are shifted downfield, relative to the precursors **1**, **2**, and **6**, while the methylenes of the neutral metal chelating dppp units remain essentially unchanged. Also observed were complex overlapping aromatic resonances for the two sets of phenyl groups of the dppp ligand for **11** and **12**, while squares **13** and **14** have signals for the methyl and methylene groups of the triethylphoshine ligands. The two sets of aromatic resonances for the 4-ethynylpyridine unit (α and β to the pyridyl nitrogen) are virtually identical. Integration of the proton signals is in accord with the requirements for **11**−**14**. The ^{19}F spectra display singlets at −79 ppm for **11** and **12**, while **13** and **14** display singlets at −75 ppm, characteristic for ionic $CF_3SO_3^-$.

Fast atom bombardment mass spectrometry (FABMS) analysis of macrocycles **9**, **11**, and **14** gave a M − 2OTf peak for **11** (1569.3 amu) with a +2 charge state (*i.e.*, separation of peaks by 0.5 *m/z*) and the M − OTf peaks at 2933.0 amu for **9** and 2756.2 amu for **14**, each with a +1 charge state (*i.e.*, separation of peaks by 1.0 *m/z*). Equally important were the isotopic distribution patterns which were consistent with the respective

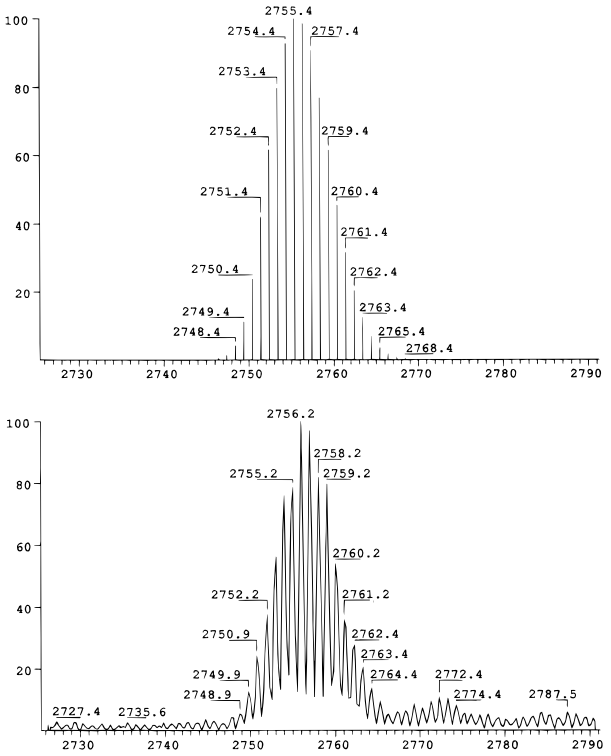

Figure 1. Calculated (top) and experimental (bottom) isotopic distribution pattern of M − OTf for **14**.

calculated compositions of these species.[10] The calculated and experimental M − OTf peak for square **14** is shown in Figure 1. The structure of **14** was unambiguously confirmed by single-crystal X-ray diffraction resulting in *ipso facto* evidence for the exact structure of these unique macrocycles and thereby also confirming the utility of FABMS for the observation of mixed neutral-charged molecular squares formed by self-assembly in solution.

Single-Crystal X-ray Molecular Structure Determinations

The geometrical features of molecular squares is of considerable interest since they represent a new and unique species of macrocycles. Continued progress in design variation of these macrocycles will prove useful for the determination of host−guest interactions and specific binding characteristics. Bond angles and cavity size are important features for the determination of potential guest size and dimension. Therefore, we attempted to obtain X-ray quality crystals of all macrocyclic squares. However, the crystals of all macrocycles described are solvent dependent, due to extensive solvent occlusion in their cavities, and collapse into amorphous material upon removal from the mother liquor. To date only macrocycle **14** gave single crystals suitable for X-ray determination; the crystallographic data for **14** is summarized in Table 1. The numbering diagram, ORTEP representation, and significant geometric features are shown in Figure 2. Selected key bond distances and angles are given in Table 2. A space filling model based on the X-ray data for square **14** using *Chem3-D Plus* is shown in Figure 3.

There are several interesting structural features observed for square **14**. The overall geometry of macrocycle **14** is nearly planar with minor deviations from a perfect square. The bonding geometry for the Pt(II) and Pd(II) centers are square planar but deviate slightly from the ideal 90° angles. The

(10) Whiteford, J. A.; Rachlin, E. M.; Stang, P. J. *Angew. Chem., Int. Ed. Engl.* **1996**, *35*, 2524−2529.

Table 1. Crystal Data and Structure Refinement

compound	molecular square **14**·5C_3H_6O
color/shape	colorless/plate
empirical formula	$C_{125}H_{158}F_{12}N_4O_{17}P_8Pd_2Pt_2$
formula weight	3195.53
T, K	173(2)
crystal system	triclinic
space group	P-1
unit cell dimensions	
a, Å	10.6859(2)
b, Å	17.4520(3)
c, Å	18.8824(1)
α, deg	85.750(1)
β, deg	88.401(1)
γ, deg	89.969(1)
V, Å^3	3510.33(9)
Z	1
ρ (calcd), Mg/m^3	1.512
μ, cm^{-1}	12.465 mm^{-1}
diffractometer/scan	Siemens SMART/CCD area detector
radiation/wavelength, Å	Mo Kα (graphite monochrom)/ 0.71073
F(000)	1612
crystal size, mm	0.10 × 0.20 × 0.20
θ range for data collection, deg	1.08−27.91
index ranges	$-9 \le h \le 14$, $-22 \le k \le 21$, $-24 \le l \le 24$
reflcns collected	22347
independent/observed reflcns	15760(R_{int} = 0.0499)/12009([$I > 2\sigma(I)$])
absorption correction	semiempirical from psi-scans
range of relat. transm. factors	0.9878 and 0.6913
refinement method	full-matrix-block least-squares on F^2
computing	SHELXTL, Ver. 5[1]
data/restraints/parameters	15752/0/833
goodness-of-fit on F^2	1.247
SHELX-93 weight parameters	0.0000, 46.1157
final R indices [$I > 2\sigma(I)$]	$R_1 = 0.0752$, $wR_2 = 0.1375$
R (all data)	$R_1 = 0.1146$, $wR_2 = 0.1672$
extinction coefficient	0.00095(10)
largest diff. peak and hole, eÅ^{-3}	1.898 and −1.926

P−Pt−P angle is 92.6° whereas the C−Pt−C angle is somewhat smaller at 88.0°. Comparison of the bond angles of coordinatively bonded macrocycles reported earlier[5e,f] reveal that the mixed organometallic-coordination complex **14** has slightly larger bond angles than the 4,4′-bipyridine Pt(II) dppp chelated macrocycle and the hybrid iodonium-Pd(II) bistriethyl phosphine macrocycle with respect to the metal corners and connecting ligands. The N−Pt−N bond angle of the 4,4′-bipyridine macrocycle is 83.9°, and the hybrid iodonium square N−Pd−N bond angle is 83.5°, whereas the N−Pd−N bond angle for macrocycle **14** is 85°. The edge-to-edge Pt−Pd distance is 9.5 Å, the diagonal Pt−Pt distance is 13.0 Å, and the diagonal Pd−Pd distance is 14.0 Å. Examination of the space filling model of **14**, which is based upon the X-ray data and shown in Figure 3, reveals a smaller cavity than one would anticipate by simply using the diagonal distances between metal corners. Considering that the van der Waals radius of Pt is ca. 1.75 Å and that of Pd is ca. 1.6 Å, the effective diagonal Pt−Pt distance is 9.5 Å, and the diagonal Pd−Pd distance is 10.8 Å. Alternatively, the approximate effective cross sectional area of the cavity of **14** is ca. 6.5 Å × 6.5 Å. The comparable cross sectional area of the all 4,4′-bipyridine Pt square is ca. 7.7 Å × 7.7 Å. The 4-ethynyl pyridine ligands of **14** are bent slightly inwards toward the center of the square. The pyridyl ligands are nearly orthogonal to the plane defined by the dppp ligand and do not display $\pi-\pi$ interaction with the phenyl rings of the dppp subunit as seen with the cationic square crystal structures previously reported.[5e,f] This can be attributed to the alkyne spacer unit in **14** which separates the dppp ligand phenyl rings from the pyridyl ring resulting in a distance too large between the two moieties to

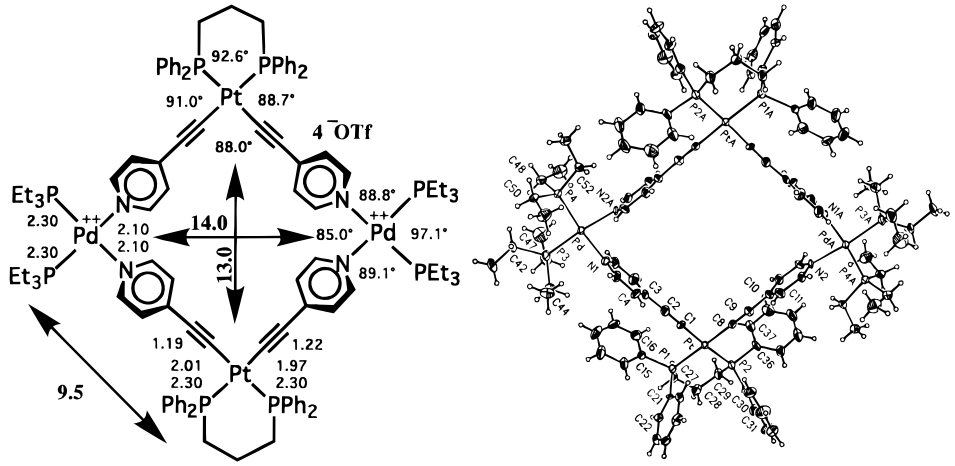

Figure 2. ORTEP representation and summary of the significant geometric features of molecular square **14**.

Table 2. Selected Bond Lengths (Å) and Angles (deg) for Molecular Square **14**

Pt−C(1)	1.972(8)	N(1)−Pd−P(3)	88.8(2)
Pt−C(8)	2.014(9)	N(2)A−Pd−P(3)	173.8(2)
Pt−P(2)	2.295(2)	N(1)−Pd−P(4)	174.1(2)
Pt−P(1)	2.297(2)	N(2)A−Pd−P(4)	89.1(2)
Pd−N(1)	2.100(7)	P(3)−Pd−P(4)	97.05(9)
Pd−N(2)A	2.106(7)	C(6)−N(1)−C(5)	117.4(8)
Pd−P(3)	2.298(2)	C(6)−N(1)−Pd	121.9(7)
Pd−P(4)	2.299(2)	C(5)−N(1)−Pd	119.5(7)
N(1)−C(6)	1.335(13)	C(13)−N(2)−C(12)	119.2(8)
N(1)−C(5)	1.337(13)	C(13)−N(2)−PdA	120.2(6)
N(2)−C(13)	1.326(12)	C(12)−N(2)−PdA	120.4(6)
N(2)−C(12)	1.331(13)	C(2)−C(1)−Pt	172.7(10)
N(2)−PdA	2.106(7)	C(1)−C(2)−C(3)	174.0(11)
C(1)−C(2)	1.223(12)	C(4)−C(3)−C(7)	117.0(9)
C(2)−C(3)	1.430(13)	C(4)−C(3)−C(2)	122.4(10)
C(3)−C(4)	1.39(2)	C(7)−C(3)−C(2)	120.6(10)
C(3)−C(7)	1.39(2)	C(5)−C(4)−C(3)	119.6(10)
C(4)−C(5)	1.375(12)	N(1)−C(5)−C(4)	123.4(10)
C(6)−C(7)	1.384(14)	N(1)−C(6)−C(7)	122.8(10)
C(8)−C(9)	1.193(13)	C(6)−C(7)−C(3)	119.7(10)
C(9)−C(10)	1.435(13)	C(9)−C(8)−Pt	179.3(9)
C(10)−C(11)	1.384(14)	C(8)−C(9)−C(10)	174.4(12)
C(10)−C(14)	1.396(14)	C(11)−C(10)−C(14)	118.2(9)
C(11)−C(12)	1.419(12)	C(11)−C(10)−C(9)	122.7(10)
C(13)−C(14)	1.391(12)	C(14)−C(10)−C(9)	119.1(10)
C(1)−Pt−C(8)	88.0(4)	C(10)−C(11)−C(12)	119.4(10)
C(1)−Pt−P(2)	174.7(3)	N(2)−C(12)−C(11)	121.2(9)
C(8)−Pt−P(2)	91.0(3)	N(2)−C(13)−C(14)	123.4(9)
C(1)−Pt−P(1)	88.7(3)	P(2)−Pt−P(1)	92.59(8)
C(8)−Pt−P(1)	175.1(3)	N(1)−Pd−N(2)A	85.0(3)

allow $\pi-\pi$ interaction. The M−P distances (2.30 Å) are normal and similar to distances obtained earlier on other macrocyclic squares. Likewise the M−N distances (2.10 Å) are normal and similar to distances on macrocyclic squares previously reported. The M−alkyne bond lengths are 1.972(8) and 2.014(9) Å, and the CC alkyne bond lengths are 1.193(13) and 1.223(12) Å for macrocycle **14**. For comparison, the previously reported average M−alkyne length of *cis*-Pt(CCO$_2$Me)(CO$_2$Et)(PPh$_3$)$_2$ is 1.991(8) Å, and the CC alkyne bond length is 1.180(11) Å.[11c] The average M−C bond length for bis(diphenylmethylphosphine)-dimethylplatinum is 2.120(4) Å.[11a] The alkyne-pyridyl-*ipso* carbon bond lengths are 1.435(13) and 1.430(13) Å which are very close to all other metal−alkyne complexes spanning a range of only 0.041 Å [1.421(8)−1.462(8) Å; d(C−C)$_{mean}$ = 1.439(9) Å] which is remarkably similar to the average bond length distribution for organic alkynes (d(C−C)$_{mean}$ = 1.435(9) Å for 55 distances with esd ≤ 0.010 Å).[11a] Importantly, very few σ bonded Pt−alkynyl crystal structures have been reported with low esd values such as seen in square **14**.[11a,b]

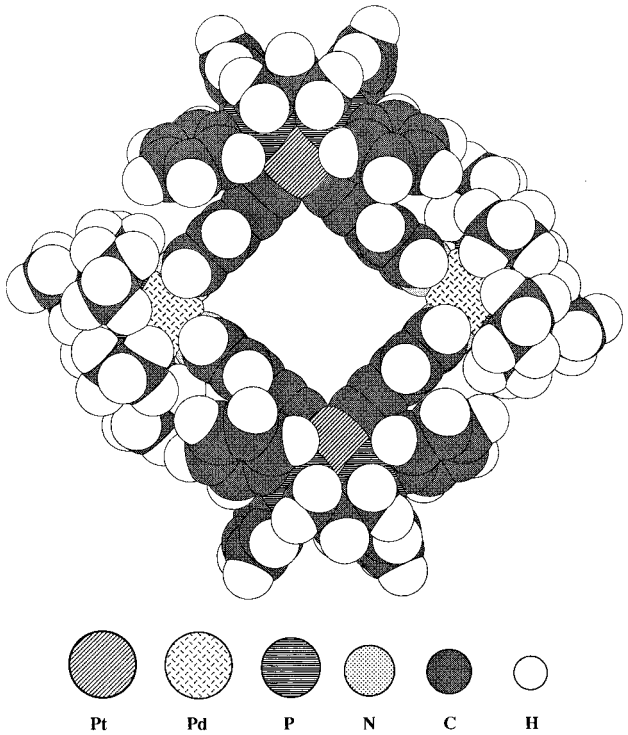

Figure 3. Space-filling model for **14** based on X-ray data.

The stacking pattern of macrocycle **14** in the solid state is shown in Figure 4. The cationic squares are stacked along the A-axis, resulting in long channel-like cavities similar to other members of the molecular square family.[5e,f] The repeating unit distance between each stacked cationic square is 10.7 Å which is larger than the hybrid-iodonium-transition metal square distance at 9.5 Å but smaller than the non-planar all transition metal 4,4′-bipyridine square distance at 15.9 Å. The one triflate counterion which is above and below the plane of the square (but outside of the square framework) was disordered and modeled by refining the triflate in two positions, each with 50% occupancy. The other triflate is between the positively charged Pd(II) center and the neutral Pt(II) center and is ordered. Acetone molecules, from the solvent, reside within square channels which propagate along the A-axis. There appear to be multiple orientations fractionally disordered for each of the

(11) (a) Manna, J.; John, K. D.; Hopkins, M. D. *Adv. Organomet. Chem.* **1995**, *38*, 79−154, and references therein. (b) Berenguer, J. R.; Forniés, J.; Lalinde, E.; Martínez, F. *J. Organomet. Chem.* **1994**, *470*, C15−C18. (c) Wisner, J. M.; Bartczak, T. J.; Ibers, J. A.; Low, J. J.; Goddard III, W. A. *J. Am. Chem. Soc.* **1986**, *108*, 347−348.

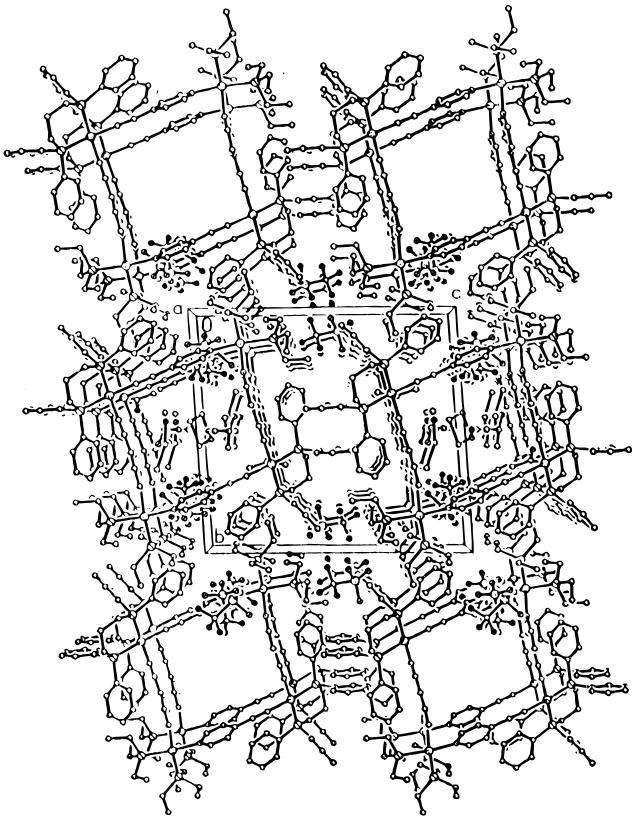

Figure 4. Stacking diagram of square **14**.

2.5 unique acetone solvent molecules per asymmetric unit (five molecules overall in the unit cell) resulting in large thermal parameters for the disordered atoms.

Chemistry of Mixed Neutral-Charged Molecular Squares

All mixed neutral-charged molecular squares synthesized to date have a C_2 axis featuring two positively charged metal centers and two neutral metal centers. It is conceivable that this type of molecular square will be suitable for binding electron-rich guests; the squares can be considered electron deficient since the datively bound metal centers each have a formal charge of +2.

Competition Experiments. It is known that nitrile groups form considerably weaker complexes with Pt and Pd than pyridine.[5f,12] In fact, mixing of 4,4′-bipyridine with a platinum-nitrile dimer resulted in exclusively the 4,4′-bipyridine tetrameric dppp complex.[5f] A similar situation was expected to exist in the case of the neutral-charged molecular squares of Pt and Pd. To test this assumption, 1 equiv of 4,4′-bipyridine was added to a representative of the mixed neutral-charged benzonitrile squares; tetramer **8**. Within 15 min of addition of 4,4′-bipyridine to square **8** in CD_2Cl_2, none of the original neutral-charged benzonitrile square **8** remained. The ^{31}P signal for the free benzonitrile dppp chelated monomer **5** was observed along with the formation of the fully charged datively bound Pd(II) 4,4′-bipyridine square reported earlier[5f] (Scheme 4). Continued interaction for about 1 h resulted in the slow precipitation of the Pd(II) 4,4′-bipyridine square while the benzonitrile monomer **5** remained in solution. These data confirm that pyridyl based squares are more stable toward electron-rich guests than nitrile based mixed neutral-charged transition metal based molecular squares and therefore likely to be more amenable to host−guest chemistry.

(12) (a) Johnson, A.; Taube, H. *J. Ind. Chem. Soc.* **1989**, *66*, 503−511. (b) Purcell, K. F.; Drago, R. S. *J. Am. Chem. Soc.* **1966**, *88*, 919−924.

Scheme 4

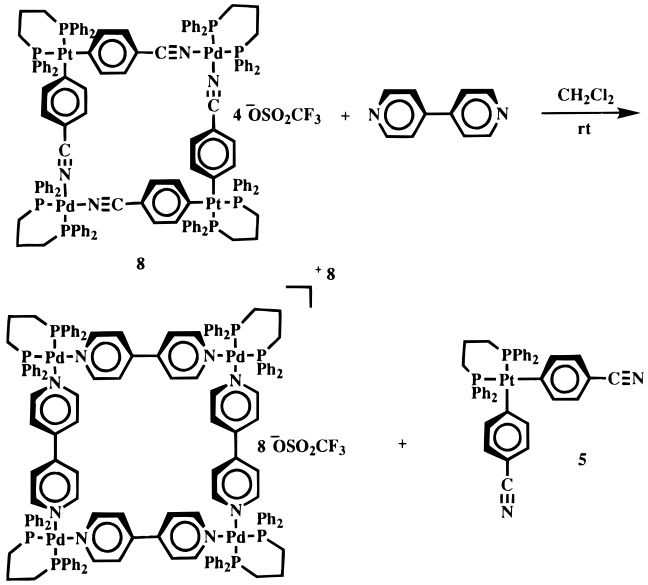

Titration Experiments. Since the gross cavity size of both the benzonitrile and 4-ethynylpyridine mixed neutral-charged macrocycles is approximately 10.8 Å × 9.5 Å diagonally and 6.5 Å × 6.5 Å from side to side (based on molecular modeling and the crystal structure for **14**), electron rich 1,4-dihydroxybenzene and 1,5-dihydroxynapthalene were chosen to test for host−guest interactions. First, a titration experiment was conducted using 1,4-dihydroxybenzene (DHB) dissolved in acetone-d_6. Square **10** was added to a solution of DHB starting with an initial ratio of 1.0:0.5 (DHB:**10**) and increasing the concentration of square **10** by increments of 0.5 equiv. The solubility of **10** only allowed for a ratio of 1.0:2.0 before the solution became saturated and square **10** began to precipitate out of solution. Neither **10** or DHB displayed a significant shift in the ^{1}H-NMR; DHB showed no change in these solutions compared with free DHB and the benzonitrile α and β protons (with respect to the Pt metal center) of **10** shifted < 0.04 ppm. A second titration experiment was conducted using 1,5-dihydroxynapthalene (DHN) dissolved in acetone-d_6 and square **10** starting with an initial ratio of 1.0:0.5 (DHN:**10**) and increasing the concentration of square **10** by increments of 0.5 equiv. This system was considerably more soluble than the previous system, and a ratio of 1.0:7.0 (DHN:**10**) was reached prior to solution saturation. A similar relationship was observed at a ratio of 1.0:2.0 where the DHN *ortho*, *meta*, and *para* protons did not change while **10** α protons shifted < 0.04 ppm. However, continued addition of **10** resulted in no shift for the DHN protons, while the α protons of **10** shifted 0.09 ppm at a ratio of 1.0:7.0 (DHN:**10**) relative to the pure square **10**.

Since DHB and DHN showed little interaction with the representative benzonitrile square **10**, square **13** was also tested with 1,5-dihydroxynapthalene to determine whether the 4-ethynylpyridine squares are suitable hosts for organic electron-rich guests. Again, little or no interaction was observed and nearly identical data to square **10** were obtained for square **13** utilizing the same titration experiments for this combination of potential host and guest.

(13) (a) Janssen, M. D.; Herres, M.; Zsolnai, L.; Spek, A. L.; Grove, D. M.; Lang, H.; van Koten, G. *Inorg. Chem.* **1996**, *35*, 2476−2483. (b) Lang, H.; Weinmann, M. *Synlett.* **1996**, 1−10. (c) Janssen, M. D. *Structural Aspects and Reactivity of Self-Assembling Organocopper and Copper Arenethiolate Aggregates*; Thesis Universiteit Utrecht, 1996; p 152. (d) Lang, H.; Blau, S.; Pritzkow, H.; Zsolnai, L. *Organometallics* **1995**, *14*, 1850−1854.

Scheme 5

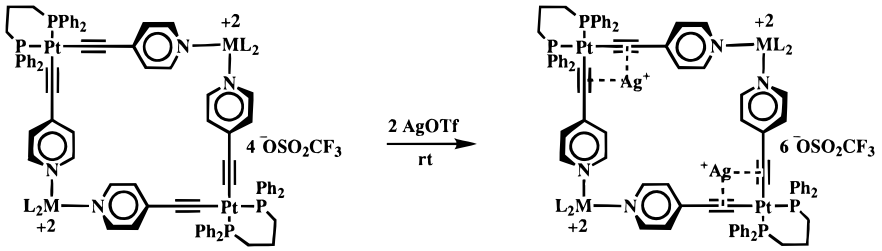

11: M = Pt, L_2=$Ph_2P(CH_2)_3PPh_2$
14: M = Pd, L=PEt_3

15: M = Pd, L=PEt_3
16: M = Pt, L_2=$Ph_2P(CH_2)_3PPh_2$

***π*-Coordination with AgOTf: The "*π*-Tweezer Effect".** After considering the binding characteristics of acetylene groups to metals such as silver, copper, and gold *via* π-interaction of the acetylene to the open coordination sites of the metal guest, as most recently demonstrated by Lang *et al.*;[13a−d] it seemed probable that 4-ethynylpyridine transition metal squares should be well suited to binding guests of this type. The bond angle between the two acetylenes on the aceylene equipped titanium example was between 87° and 91° upon interaction with the given metal guest.[13d] Since the crystal structure of molecular square **14** revealed a bond angle of 88° between the two acetylenes, it should function effectively as a host for silver *via* the π-tweezer effect. Furthermore, the molecular squares are particularly interesting since they have two of these binding units per square (*i.e.* two neutral dpppPt−bis-ethynylpyridine centers) and should be able to complex 2 equiv of a silver complex (Scheme 5). Attempts to bind one equiv of silver triflate to **11** or **14** failed, resulting only in a mixture of several products which rapidly formed an insoluble precipitate after about 20 min. Interaction of square **14** with 2 equiv of silver triflate in acetone-d_6 did indeed show significant shift differences in the ^{31}P, ^{13}C, ^{1}H NMR, and IR spectra. Particularly diagnostic for the formation of complex **15** was the shift in the ^{31}P NMR singlet where the neutral Pt corner containing the acetylene ligands shifted ∼2.6 ppm upfield with a coupling constant increase of 167 Hz. This upfield shift and coupling constant increase can be attributed to the change of the angle beween the two acetylene ligands upon complexation, thus affecting the angle of the two phosphines of the dppp ligand with respect to the metal center.[14] As expected the Pd center phosphines are less affected by the Ag complexation, and, therefore, the ^{31}P shift was not as significant (0.03 ppm downfield). The α and β protons of the pyridyl (with respect to the pyridine nitrogen) resulted in further downfield shifts of 0.15 and 0.11 ppm, respectively, upon complexation with AgOTf. The ^{13}C data show significant shifts particularly with respect to the *ipso* carbon on the pyridyl (3.5 ppm upfield) and the β alkyne carbon which shifted 2.4 ppm downfield with respect to the pure square **14**. The IR spectrum also confirmed AgOTf complexation, thus, the alkyne CC stretch shifted to smaller wavenumbers (2091 cm^{-1}, $\delta = 34$ cm^{-1}). This is caused by two electron backdonation of each alkyne to the silver.[13a] Square **11** showed similar shifts in the ^{31}P NMR upon complexation of 2 equiv of AgOTf (Pt−Pt 4-ethynylpyridine square-silver triflate complex **16**) where the neutral Pt corner containing the acetylene ligands shifted 3.2 ppm upfield with a coupling constant increase of 151 Hz. The charged Pt center phosphines are also less affected by the Ag complexation, and, therefore, the ^{31}P shift was not as significant (0.14 ppm downfield, coupling constant increase of 22 Hz). The α and β protons of the pyridyl (with respect to the pyridine nitrogen) shift 0.06 downfield and 0.01 ppm upfield, respectively, upon Ag^+ complexation. The IR spectrum exhibited a single alkyne stretch shifted to smaller wavenumbers (2081 cm^{-1}, $\delta = 33$ cm^{-1}). Both squares **11** and **14** displayed an absorption band in the UV−vis spectra at $\lambda_{max} = 324$ nm. A small blue shift was observed for the respective silver complexes **16** and **15** (λ_{max} = 314 and 318 nm, respectively). The most compelling evidence for the coordination of AgOTf is the observation by FABMS of the M − OTf base peak at 3799.9 amu (Figure 5) and the M − 2OTf peak (+2 charge state) at 1824.0 amu with isotopic distributions essentially equiv to the calculated patterns confirming the 2:1 stoichiometry of the silver guest to the square **11**. The M − OTf peak for **16** was separated by 1 *m/z* unit, as expected, indicating the +1 charge state of this macrocyclic fragment resulting from the loss of one triflate counterion out of a total of six. The M − 2OTf peak charge state of +2 was indicated by the 0.5 *m/z* separation of the peaks of the isotopic distribution pattern of the fragment observed. FABMS studies of the more labile Pt−Pd 4-ethynylpyridine square-silver triflate complex **15** resulted in a homolytic cleavage of the host−guest complex into two equal halves and loss of one triflate per half as indicated by the +1 charge state and the *m/z* value observed (1559.3 amu).

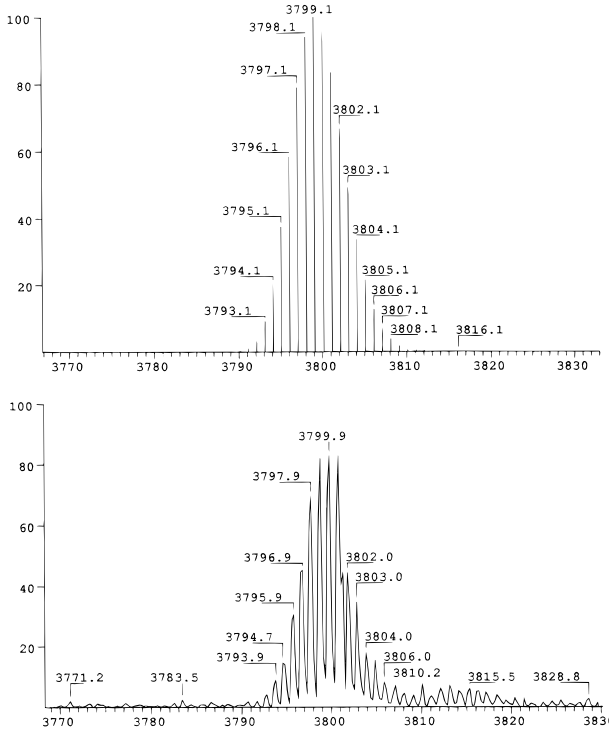

Figure 5. Calculated (top) and experimental (bottom) isotopic distribution pattern of M − OTf for **16**.

(14) (a) Wrackmeyer, B.; Horchler, K. In *Progress in NMR Spectroscopy*: *NMR Parameters of Alkynes*; Pergamon Press: Great Britain, 1990; pp 209−253. (b) Morris, D. G. In *The Chemistry of Functional Groups, Supplement C*: *NMR Spectra of Acetylenes*; Patai, S., Rappoport, Z.; Eds.; John Wiley & Sons Ltd.: New York, 1983; pp 1035−1056.

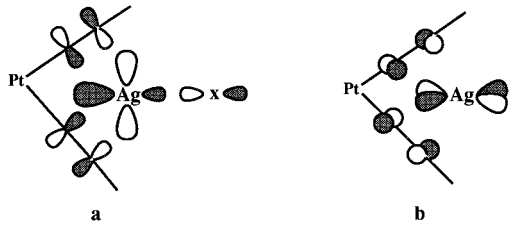

Figure 6. Metal-to-ligand (back-) donation.

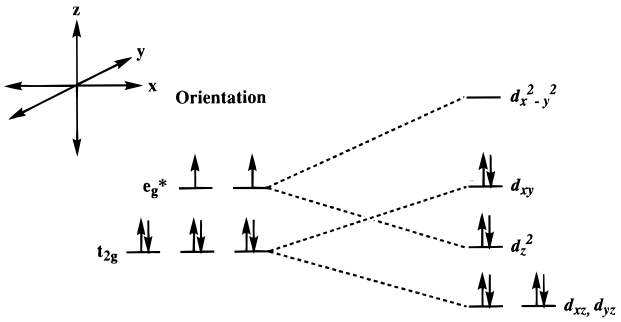

Figure 7. Energy levels for square planar platinum(II) complexes.

As discussed by Lang *et al*.,[13b] the alkyne−metal interaction can arise from a σ donation of electron density from a filled π orbital on the alkyne to the empty sp hybrid on Ag and a back-donating component resulting from the donation of electon density from filled d orbitals on the metal to empty π* orbitals on the alkyne as shown in Figure 6. EHT (Extended Hückel Theory) analysis by van Koten[13a,c] *et al*. of the $Cp_2Ti(CCH)_2CuCH_3$ model system indicated that the back bonding component in the alkyne-to-MR interaction is more important. They found that two combinations of π* alkyne orbitals possess both suitable symmetry and energy to provide efficient interactions with a filled Cu^I (Ag^I) orbital (ds mixture). The first interaction (Figure 6a) takes place in the plane of the $Ti(CCH)_2Cu-R$, while the second interaction (Figure 6b) occurs perpendicular to this plane. The typical crystal field model for a square planar metal system (Figure 7) shows the d_{xy} component at a higher energy level through π interaction with both acetylene π* orbitals than the degenerate d_{xz} and d_{yz} orbitals which are capable of interacting with only one ligand per d orbital since the ligands of a square planar complex lie along the *x* and *y* axis (point directly at the $d_{x^2-y^2}$ orbitals). It can also be reasoned that the effect on the the Pt system is less than the Ti system since Pt σ bonded ligands are more covalently bonded when compared to the Ti σ bonded ligands which are considered to have more ionic character.[15]

Conclusions

A total of eight novel homo and heteronuclear mixed neutral-charged organometallic macrocyclic squares have been synthesized *via* modular self-assembly featuring benzonitrile ligands or 4-ethynylpyridine ligands with two types of Pt and Pd phoshine ligands (dppp and triethylphoshine). The X-ray crystal structure of **14** revealed a planar slightly rhomboid geometry and bond angles that are <90°. As expected the benzonitrile based squares are more labile than the 4-ethynylpyridine based squares as determined by the addition of 1 equiv of 4,4′-bipyridine. Neither the benzonitrile or the 4-ethynylpyridine based squares showed a strong affinity for neutral electron-rich aromatics such as 1,4-dihydroxybenzene or 1,5-dihydroxynaphthalene. The organometallic squares incorporating acetylene groups are functionally and geometrically well suited to binding simple silver guests such as silver triflate. Thus, addition of 2 equiv of silver triflate to the 4-ethynylpyridine based Pt−Pt and Pt−Pd squares clearly shows host−guest interaction presumably *via* the π-tweezer effect. The 88° angle between the acetylene moieties in the free Pt−Pd square, as determined by X-ray crystallography, allow for the inclusion of two silver atoms (one per neutral corner) to the 4-ethynylpyridine based molecular squares. Significant shift values in the ^{31}P, ^1H, ^{13}C NMR, and IR support the proposed inclusion phenomenon for the 4-ethynylpyridine based Pt−Pt and Pt−Pd organometallic squares. FABMS studies confirmed the 1:2 host:guest stoichiometry for the Pt−Pt host:silver triflate guest complex **16** by observation of the M − OTf species with a +1 charge state and the M − 2OTf species with a +2 charge state for complex **16**. It is known that silver, coordinated to acetylenes, can also bind to other species such as alkynyl and aryl moieties.[13a] Thus it is likely that these molecular squares containing silver guests may be further elaborated by the addition of other ligands to Ag^+. These studies are under active investigation.

Experimental Section

General Methods. Melting points (uncorrected) were obtained with a Mel-Temp capillary melting point apparatus. Infrared spectra were recorded as CCl_4 mulls on a Mattson FT-IR spectrometer. All NMR spectra were recorded on a Varian XL 300, Varian Unity 300, or a Varian VXR 500 spectrometer. The ^1H NMR spectra were recorded at 300 MHz, and chemical shifts are reported relative to the residual protonated solvent peaks of CD_2Cl_2 δ 5.32, and acetone-d_6 δ 2.05. The ^{13}C NMR spectra were recorded at 75 or 125 MHz, ^1H decoupled, and reported relative to CD_2Cl_2 δ 54.0 or acetone-d_6 δ 29.93. The ^{19}F NMR spectra were recorded at 282 MHz, and chemical shifts were reported relative to external $CFCl_3$ δ 0.0 (sealed capillary) in the appropriate deuterated solvent. The ^{31}P NMR spectra were recorded at 121 MHz, ^1H decoupled, and reported relative to external 85% H_3PO_4 (sealed capillary) in the appropriate deuterated solvent.

Mass spectra were obtained with a Finnigan MAT 95 mass spectrometer with a Finnigan MAT ICIS II operating system under positive fast atom bombardment (FAB) conditions at 8 keV. 3-Nitrobenzyl alcohol was used as a matrix in CH_2Cl_2 or acetone as solvent, polypropylene glycol, and cesium iodide were used as a references for peak matching. Microanalyses were performed by Atlantic Microlabs, Atlanta, GA.

Materials. All commercial reagents were ACS reagent grade and used without further purification or after sublimation. Reagent grade methylene chloride was dried by distillation over CaH_2. Diethyl ether and THF were distilled from Na/benzophenone. Acetone was refluxed over $KMnO_4$, distilled, and handled under nitrogen. HPLC grade benzene, toluene, and pentane were dried over molecular sieves and used without further purification. Reaction flasks were flame-dried and flushed with argon prior to use with schlenk techniques unless otherwise noted. Trimethylsilyl acetylene, diphenylphosphinopropane, silver triflate, 2.5 M *n*-butyllithium in hexanes, and 1.7 M *tert*-butyllithium in pentane were purchased from Aldrich. Pd(II)dichloride was purchased from Lancaster. The free 4-bromopyridine was obtained by deprotonation of the hydrochloride salt with triethylamine in diethyl ether at rt overnight in the absence of light. It is unstable and so was generated immediately before use.

4-Ethynylpyridine. 4-Ethynylpyridine was synthesized by a modified Castro−Stevens coupling.[9b] To a solution of trimethylsilyl acetylene (3.28 g, 33.4 mmol) in 60 mL of THF under argon, was added triethylamine (3.63 g, 35.9 mmol), 4-bromopyridine (5.27g, 33.4 mmol), copper iodide (508 mg, 2.67 mmol), and palladium tetrakis-(triphenylphosphine) (2.90 g, 2.5 mmol), and the reaction mixture subsequently stirred overnight in the absence of light. The solvent was removed *via* rotary evaporation, and then the residue was extracted with diethyl ether (4 × 50 mL). The ether extracts were washed with saturated NaCl, dried over $MgSO_4$, and filtered, and the solvent was removed *via* rotary evaporation to afford the crude trimethylsilyl-4-

(15) Waters, J. A.; Mortimer, G. A. *J. Organomet. Chem.* **1970**, *22*, 417−424.

alkynylpyridine. Desilylation of this material was achieved by treatment with 1.0 M 40 mL of THF with TBAF (35 mL, 35.0 mmol), in THF (40 mL) at 0 °C for 6 h. Removal of the solvent *via* rotary evaporation and sublimation of the residue (80 °C, 1 mmHg) resulted in transparent colorless crystals (1.75 g, 50% overall yield). Physical characteristics were consistent with previously reported data.[9a]

***cis*-Pt(dppp)(4-benzonitrile)$_2$ (5).** A solution of *n*-BuLi (2.5 M, hexanes, 1.77 mmol) was added *via* syringe to a solution of 4-iodobenzonitrile (4.05 mg, 1.77 mmol) in 10 mL of Et_2O at −78 °C under argon. Platinum(II) dichloride (dppp) (300 mg, 0.44 mmol) was immediately added in one portion at −78 °C. The cold bath was removed, and the reaction mixture was allowed to warm to 25 ˚C on its own and allowed to stir for 5 h at 25 °C followed by solvent removal *via* rotary evaporation at ambient temperature. The residue was extracted with toluene (3 × 25 mL). The extracts were combined, and the solvent was removed *via* rotary evaporation. The residue was dissolved in 4 mL of CH_2Cl_2. Crystallization was induced by addition of diethyl ether and pentane resulting in yellow crystals (350 mg, 83%): mp 196−199 °C dec; IR (CCl_4) 3077, 3061 (Ar), 2939 (CH_2), 2212 (CN) cm^{-1}; ^{1}H NMR (CD_2Cl_2) δ 7.50−7.26 (m, 20H), 7.14 (m, 4H), 6.74 (m, 4H), 2.67 (bs, 4H), 1.88 (m, 2H); ^{13}C{^{1}H} NMR (CH_2Cl_2) δ 133.3 (C*o*), 130.5 (C_p), 128.5 (C_m), 131.7 (Pt−P−C_{ipso}), 129.5 (C_α), 136.9 (C_β), 120.8 (C_{ipso}), 172.4 ((Pt−$C_{ipso'}$), $^2J_{P-C}$ = 96.0 Hz), 104.1 (CN), 26.3 (Pt−P−CH_2), 19.5 (CH_2); ^{31}P{^{1}H} NMR (CD_2Cl_2) δ 0.69 (J_{Pt-P} = 1740 Hz).

Cyclobis[[*cis*-Pt(dppp)(4-benzonitrile)$_2$][*cis*-Pt^{2+}(dppp)2$^-$-OSO$_2$CF$_3$]] (7). To a solution of monomer **5** (0.0370 mmol) in 10 mL of CH_2Cl_2 was added Pt(dppp)(OTf)$_2$ **1** (33.5 mg, 0.0370 mmol) all at once at 25 °C and stirred for 15 min. The solvent volume was decreased to 1 mL *via* rotary evaporation. Crystallization was induced by addition of diethyl ether and pentane, resulting in light pink crystals (57.2 mg, 90%): mp 210−213 °C dec; IR (CCl_4) 3055 (Ar), 2976, 2928, 2865 (CH_2), 2256 (CN), 1224, 1150, 1102, 1029 (OTf) cm^{-1}; ^{1}H NMR (CD_2Cl_2) δ 7.30−7.18 (m, 80H), 7.00 (m, 8H), 6.25 (m, 8H), 2.97 (bs, 8H), 2.63 (m, 8H), 2.24 (m, 4H), 1.87 (m, 4H); ^{13}C{^{1}H} NMR (CH_2Cl_2) δ 133.4 (Pt−P−C*o*), 131.2 (Pt−P−C_{ipso}), 130.7 (Pt−P−C_p), 128.5 (Pt−P−C_m), 133.2 (Pt′−P−C_o), 133.1 (Pt′−P−C*p*), 129.9 (Pt′−P−C*m*), 124.5 (Pt′−P−C_{ipso}), 180.4 ((Pt′−$C_{ipso'}$), $^2J_{P-C}$ = 92.7 Hz), 137.3 (Pt−C_β), 129.8 (Pt−C_α), 123.9 (Pt−C_{ipso}), 121.4 (q, J_{C-F} = 321 Hz, OTf), 97.5 (CN), 26.1 (Pt−P−CH_2), 21.7 (Pt′−P−CH_2), 19.6 (CH_2), 18.6 (CH′$_2$); ^{31}P{^{1}H} NMR (CD_2Cl_2) δ −0.21 (s, J_{Pt-P} = 1773 Hz), −12.2 (s, J_{Pt-P} = 3349 Hz); ^{19}F NMR (CD_2Cl_2) δ −79. Anal. Calcd for $Pt_4C_{140}H_{116}P_8S_4N_4O_{12}F_{12}$·$CH_2Cl_2$: C, 48.12; H, 3.49; N, 1.59; S, 3.64. Found: C, 47.93; H, 3.61; N, 1.55; S, 3.75.

Cyclobis[[*cis*-Pt(dppp)(4-benzonitrile)$_2$][*cis*-Pd^{2+}(dppp)2$^-$-OSO$_2$CF$_3$]] (8). To a solution of monomer **5** (44.0 mg 0.054 mmol) in 10 mL of CH_2Cl_2 was added Pd(dppp)(OTf)$_2$ **2** (44.3 mg, 0.054 mmol) all at once at 25 °C, and the solution was stirred for 15 min. The solvent volume was decreased to 3 mL *via* rotary evaporation. Crystallization was induced by addition of diethyl ether and pentane, resulting in reddish brown crystals (85.0 mg, 96%): mp 169−173 °C dec; IR (CCl_4) 3057 (Ar), 2918 (CH_2), 2249 (CN), 1276, 1152, 1101, 1029 (OTf) cm^{-1}; ^{1}H NMR (CD_2Cl_2) δ 7.64−7.25 (m, 80H), 7.20 (m, 8H), 6.42 (m, 8H), 2.88 (bs, 8H), 2.68 (bs, 8H), 2.30 (m, 4H), 1.90 (m, 4H); ^{13}C{^{1}H} NMR (CD_2Cl_2) δ 133.3 (Pt−P−C*o*), 131.1 (Pt−P−C_{ipso}), 130.6 (Pt−P−C_p), 128.5 (Pt−P−C_m), 133.2 (Pd−P−C_o), 133.1 (Pd−P−C*p*), 129.9 (Pd−P−C*m*), 125.2 (Pd−P−C_{ipso}), 124.2 (m, C_{ipso}), 137.2 (Pt−C_β), 129.8 (Pt−C_α), 178.6 (q, Pt−C_{ipso}, ($^2J_{P-C}$ = 99.4Hz)), 121.3 (q, J_{C-F} = 321 Hz, OTf), 98.9 (m, CN), 26.1 (Pt−P−CH_2), 21.8 (Pd−P−CH_2), 19.5 (CH_2), 18.8 (CH′$_2$); ^{31}P{^{1}H} NMR (CD_2Cl_2) δ 13.6-(s), −0.29 (s, J_{Pt-P} = 1765 Hz); ^{19}F NMR (CD_2Cl_2) δ −79. Anal. Calcd for $Pt_2Pd_2C_{140}H_{116}P_8S_4N_4O_{12}F_{12}$: C, 51.62; H, 3.71; N, 1.72; S, 3.94. Found: C, 51.33; H, 3.85; N, 1.68; S, 3.94.

Cyclobis[[*cis*-Pt(dppp)(4-benzonitrile)$_2$][*cis*-Pt^{2+}(PEt$_3$)$_2$2$^-$-OSO$_2$CF$_3$]] (9). To a solution of monomer **5** (151 mg, 0.186 mmol) in 8.6 mL of acetone was added Pt(PEt$_3$)$_2$(OTf)$_2$ **3** (136 mg, 0.186 mmol) all at once at 25 °C, and the solution was stirred for 4 h. The solvent volume was decreased to 4 mL *via* rotary evaporation. Crystallization was induced by addition of diethyl ether and pentane, resulting in white crystals (262 mg, 91%): mp 195−197 °C dec; IR (CCl_4) 3044 (Ar), 2974, 2937 (CH_2, CH_3), 2259 (CN), 1260, 1146, 1101, 1029 (OTf) cm^{-1}; ^{1}H NMR (acetone-d_6) δ 7.61−7.50 (m, 16H, *o*), 7.35 (m, 32H, *m*, *p*, α), 6.99 (m, 8H, $^3J_{HH}$ = 4.8 Hz, *β*), 2.33 (m, 24H), 1.90 (m, 4H), 1.31 (m, 36H); ^{13}C{^{1}H} NMR (acetone-d_6) δ 134.1 (Pt−P−C_o), 132.3 (Pt−P−C_{ipso}), 131.1 (Pt−P−C_p), 129.2 (Pt−P−C_m), 137.2 (Pt−C_β), 129.8 (Pt−C_α), 124.9 (m, C_{ipso}), 122.3 (q, J_{C-F} = 322 Hz, OTf), 98.7 (m, CN), 26.1 (Pt−P−CH_2), 21.8 (Pd−P−CH_2), 19.5 (CH_2), 18.8 (CH′$_2$); ^{31}P{^{1}H} NMR (acetone-d_6) δ 11.8 (s, J_{Pt-P} = 3404 Hz), 2.7 (s, J_{Pt-P} = 1774 Hz); ^{19}F NMR (acetone-d_6) δ −75. Anal. Calcd for $Pt_2Pd_2C_{140}H_{116}P_8S_4N_4O_{12}F_{12}$: C, 42.86; H, 4.19; N, 1.82; S, 4.16. Found: C, 42.95; H, 4.46; N, 1.78; S, 3.96; FAB LRMS, *m/z* 2933.0 (M − OTf)

Cyclobis[[*cis*-Pt(dppp)(4-benzonitrile)$_2$][*cis*-Pd^{2+}(PEt$_3$)$_2$2$^-$-OSO$_2$CF$_3$]] (10). To a solution of monomer **5** (153 mg, 0.189 mmol) in 8.6 mL acetone was added Pd(PEt$_3$)$_2$(OTf)$_2$ **4** (121 mg, 0.189 mmol)-all at once at 25 °C and stirred for 1 h. The solvent volume was decreased to 4 mL *via* rotary evaporation. Crystallization was induced by addition of diethyl ether and pentane, resulting in yellow crystals (258 mg, 94%): mp 137−139 °C dec; IR (CCl_4) 3057 (Ar), 2976, 2941 (CH_2CH_3), 2255 (CN), 1256, 1150, 1101, 1029 (OTf) cm^{-1}; ^{1}H NMR (acetone-d_6) δ 7.57−7.52 (m, 16H, *o*), 7.38−7.32 (m, 24H, *m*, *p*), 7.21 (m, 8H, *β*), 6.77 (m, 8H, α) 2.91 (bs, 8H), 2.31−2.20 (m, 24H), 1.88 (m, 4H), 1.40−1.29 (m, 36H); ^{13}C{^{1}H} NMR (acetone-d_6) δ 134.1 (Pt−P−C*o*), 132.6 (Pt−P−C_{ipso}), 131.1 (Pt−P−C_p), 129.1 (Pt−P−C_m), 138.0 (Pt−C_β), 130.0 (Pt−C_α), 122.7 (C_{ipso}), 121.9 (q, J_{C-F} = 321 Hz, OTf), 102.6 (m, CN), 26.2 (m, Pt−P−CH_2), 19.9 (bs, CH_2), 17.3 (m, Pd−P−CH_2CH_3), 8.8 (bs, Pd−P−CH_2CH_3); ^{31}P{^{1}H} NMR (acetone-d_6) δ 51.8 (s), 2.9 (s, J_{Pt-P} = 1763 Hz); ^{19}F NMR (acetone-d_6) δ −75. Anal. Calcd for $Pt_2Pd_2C_{110}H_{128}P_8S_4N_4O_{12}F_{12}$: C, 45.48; H, 4.44; N, 1.93; S, 4.41. Found: C, 45.19; H, 4.45; N, 1.90; S, 4.25.

***cis*-Pt(dppp)(4-ethynylpyridine)$_2$ (6).** A solution of *t*-BuLi (1.7 M, hexanes, 1.97 mmol) was added *via* syringe to a solution of 4-alkynylpyridine (202 mg, 1.97 mmol) in 80 mL of THF at −78 °C under argon. Platinum(II) dichloride (dppp) (666 mg, 0.98 mmol) was immediately added all at once at −78 °C. The cold bath was removed, and the reaction mixture was allowed to warm to 25 °C on its own and stirred for 5 h without light followed by solvent removal *via* rotary evaporation at ambient temperature. The residue was extracted with benzene (4 × 40 mL). The extracts were combined, and the solvent was removed *via* rotary evaporation. The residue was dissolved in 4 mL of CH_2Cl_2. Crystallization was induced by addition of diethyl ether and pentane resulting in white crystals (544 mg, 68%): mp 221−223 °C dec; IR (CCl_4) 3057, 3037 (Ar), 2944, 2929 (CH_2), 2121 (CC) cm^{-1}; ^{1}H NMR (CD_2Cl_2) δ 8.20 (d, 4H, $^3J_{HH}$ = 6.1 Hz), 7.75−7.68 (m, 8H), 7.43−7.36 (m, 12H), 6.62 (d, 4H, $^3J_{HH}$ = 6.1 Hz), 2.56 (m, 4H), 2.04 (m, 2H); ^{13}C{^{1}H} NMR (CH_2Cl_2) δ 134.0 (C*o*), 131.4 (C_p), 129.0 (C_m), 131.2 (Pt−P−C_{ipso}), 149.4 ($C_{\alpha pyr}$), 125.8 ($C_{\beta pyr}$), 135.7 ($C_{ipso pyr}$), 114.4 (q, CC−Pt$_\alpha$, $^2J_{P-C(cis)}$ = 21.1 Hz, $^2J_{P-C(trans)}$ = 124 Hz), 104.1 (t, CC−Pt$_\beta$, $^2J_{P-C}$ = 17.4 Hz) 26.3 (Pt−P−CH_2), 19.5 (CH_2); ^{31}P{^{1}H} NMR (CD_2Cl_2) δ −3.1 (s, J_{Pt-P} = 2185 Hz); FAB LRMS, *m/z* 812.2 (M + H).[10]

Cyclobis[[*cis*-Pt(dppp)(4-ethynylpyridine)$_2$][*cis*-Pt^{2+}(dppp)2$^-$-OSO$_2$CF$_3$]] (11). To a solution of monomer **6** (70.0 mg, .086 mmol) in 7.2 mL of CH_2Cl_2 was added Pt(dppp)(OTf)$_2$ **1** (78.1 mg, 0.012 mmol) all at once at 25 °C, and the solution was stirred for 4 h. The solvent volume was decreased to 4 mL *via* rotary evaporation. Crystallization was induced by addition of diethyl ether and pentane, resulting in white crystals (141 mg, 95%): mp 211−213 °C dec; IR (CCl_4) 3051 (Ar), 2991, 2927, 2855 (CH_2), 2114 (CC), 1224, 1156, 1103, 1029 (OTf) cm^{-1}; UV−vis (CH_2Cl_2) λ_{max} = 318 nm, ϵ = 9.9 × 10^4 L cm^{-1} mol^{-1}; ^{1}H NMR (CD_2Cl_2) δ 8.20 (d, 8H, $^3J_{HH}$ = 5.4 Hz), 7.70−7.20 (m, 80H), 6.28 (d, 8H, $^3J_{HH}$ = 6.4 Hz), 3.2 (bs, 8H), 2.5 (bs, 8H), 2.10 (m, 8H); ^{13}C{^{1}H} NMR (CH_2Cl_2) δ 133.9 (Pt−P−C_o), 131.0 (Pt−P−C_{ipso}), 131.7 (Pt−P−C_p), 129.1 (Pt−P−C_m), 133.5 (Pt′−P−C_o), 132.5 (Pt′−P−C_p), 129.7 (Pt′−P−C_m), 125.3 (Pt′−P−C_{ipso}), 148.9 ($C_{\alpha pyr}$), 128.5 ($C_{\beta pyr}$), 139.2 ($C_{ipso pyr}$), 124.0 (q, J_{Pt-C} = 122 Hz, CC−Pt$_\alpha$), 106.8 (t, $^2J_{Pt-C}$ = 16.7 Hz, (CC−Pt$_\beta$)), 121.8 (q, J_{C-F} = 321 Hz, OTf), 26.0 (Pt−P−CH_2), 21.8 (Pt′−P−CH_2), 20.6 (CH_2), 18.2 (CH′$_2$); ^{31}P{^{1}H} NMR (CD_2Cl_2) δ −3.0 (s, J_{Pt-P} = 2204 Hz), −11.0 (s, J_{Pt-P} = 3035 Hz); ^{19}F NMR (CD_2Cl_2) δ −76. Anal. Calcd for $Pt_4C_{140}H_{120}P_8S_4N_4O_{12}F_{12}$: C, 48.96; H, 3.52; N, 1.63. Found: C, 49.03; H, 3.60; N, 1.65; FAB LRMS, *m/z* 1569.2 (M − 2OTf).[10]

Cyclobis[[*cis*-Pt(dppp)(4-ethynylpyridine)$_2$][*cis*-Pd^{2+}(dppp)2$^-$-OSO$_2$CF$_3$]] (12). To a solution of monomer **6** (78.2 mg, 0.096 mmol)

in 6.7 mL of CH_2Cl_2 was added Pd(dppp)$(OTf)_2$ **2** (78.7 mg, .014 mmol) all at once at 25 °C, and the solution was stirred for 1 h. The solvent volume was decreased to 4 mL *via* rotary evaporation. Crystallization was induced by addition of diethyl ether and pentane, resulting in yellow crystals (156 mg, 99%): mp 260−263 °C dec; IR (CCl_4) 3061 (Ar), 2958, 2928, 2921 (CH_2), 2113 (CC), 1223, 1154, 1101, 1028 (OTf) cm^{-1}; ^1H NMR (CD_2Cl_2) δ 8.19 (d, 8H, $^3J_{HH}$ = 6.3 Hz), 7.70−7.20 (m, 80H), 6.25 (d, 8H, $^3J_{HH}$ = 5.9 Hz), 3.08 (bs, 8H), 2.51 (bs, 8H), 2.05 (m, 8H); $^{13}C\{^1H\}$ NMR (CH_2Cl_2) δ 133.9 (Pt−P−C*o*), 131.1 (Pt−P−C_{ipso}), 131.7 (Pt−P−C_p), 129.0 (Pt−P−C_m), 133.4 (Pd−P−C_o), 132.5 (Pd−P−C_p) ,129.8 (Pd−P−C_m), 126.0 (Pd−P−C_{ipso}), 148.9 ($C_{\alpha pyr}$), 128.1 ($C_{\beta pyr}$), 138.7 ($C_{ipso pyr}$), 122.6 (q, CC−Pt_{α}, J_{P-C} = 124 Hz), 106.8 (t, CC−Pt_{β}, $^2J_{P-C}$ = 15.9 Hz), 121.7 (q, J_{C-F} = 321 Hz, OTf), 25.6 (m, Pt−P−CH_2), 19.7 (bs, CH_2), 16.8 (m, Pt−P−*CH_2*CH_3), 8.6 (bs, Pt−P−CH_2*CH_3*); $^{31}P\{^1H\}$ NMR (CD_2Cl_2) δ −3.1 (s, J_{Pt-P} = 2202 Hz), 10.3 (s); ^{19}F NMR (CD_2Cl_2) δ −76. Anal. Calcd for $Pt_2Pd_2C_{140}H_{120}P_8S_4N_4O_{12}F_{12}\cdot CH_2Cl_2$: C, 50.67; H, 3.68; N, 1.68; S, 3.84. Found: C, 50.84; H, 3.81; N, 1.80; S, 3.96.

Cyclobis[[*cis*-Pt(dppp)(4-ethynylpyridine)$_2$][*cis*-Pt^{2+}(PEt$_3$)$_2$2$^-$-OSO$_2$CF$_3$]] (13). To a solution of monomer **6** (40.3 mg, 0.050 mmol) in 2.7 mL of acetone was added $Pt(PEt_3)_2(OTf)_2$ **3** (36.2 mg, 0.050 mmol) all at once at 25 °C, and the solution was stirred for 4 h . Crystallization was induced by addition of diethyl ether and pentane, resulting in white crystals (72 mg, 94%): mp 321−324 °C dec; IR (CCl_4) 3056 (Ar), 2971, 2937 (CH_2CH_3) 2944, 2929 (CH_2, CH_3), 2116 (CC), 1223, 1161, 1106, 1029 (OTf) cm^{-1}; ^1H NMR (acetone-d_6) δ 8.66 (d, 8H, $^3J_{HH}$ = 5.6 Hz), 7.70−7.63 (m, 16H, *o*),7.43−7.37 (m, 24H, *m*, *p*), 6.75 (d, 8H, $^3J_{HH}$ = 6.0 Hz), 2.91 (bs, 8H), 2.10−2.00 (obscured, m, 8H), 2.00−1.85 (m, 24H), 1.40−1.24 (m, 36H); $^{13}C\{^1H\}$ NMR (acetone-d_6) δ 134.4 (Pt−P−C*o*), 131.3 (Pt−P−C_{ipso}), 131.9 (Pt−P−C_p), 129.3 (Pt−P−C_m), 150.0 ($C_{\alpha pyr}$), 129.2 ($C_{\beta pyr}$), 141.0 ($C_{ipso pyr}$), 131.8−131.2 (obscured, q, $^2J_{P-C(cis)}$ = 20.5 Hz, CC−Pt_{α}), 108.0 (t, $^2J_{P-C}$ = 17.6 Hz, CC−Pt_{β}), 121.8 (q, J_{C-F} = 322 Hz, OTf), 24.8 (m, Pt−P−CH_2), 20.1 (bs, CH_2), 15.6 (m, Pt−P−*CH_2*CH_3), 8.2 (bs, Pt−P−CH_2*CH_3*); $^{31}P\{^1H\}$ NMR (acetone-d_6) δ 3.8 (s, J_{Pt-P} = 3067 Hz), −2.3 (s, J_{Pt-P} = 2174 Hz); ^{19}F NMR (acetone-d_6) δ −75. Anal. Calcd for $Pt_4C_{110}H_{128}P_8S_4N_4O_{12}F_{12}\cdot 2OC(CH_3)_2$: C, 43.56; H, 4.30; N, 1.78; S, 4.01. Found: C, 43.64; H, 4.27; N, 1.87; S, 4.17.

Cyclobis[[*cis*-Pt(dppp)(4-ethynylpyridine)$_2$][*cis*-Pd^{2+}(PEt$_3$)$_2$2$^-$-OSO$_2$CF$_3$]] (14). To a solution of monomer **6** (40.3 mg, 0.050 mmol) in 3.0 mL acetone was added $Pd(PEt_3)_2(OTf)_2$ **4** (31.8 mg, 0.050 mmol)-all at once at 25 °C, and the solution was stirred for 1 h. Crystallization was induced by addition of pentane, resulting in yellow crystals (70 mg, 97%): mp 208−211 °C dec; IR (CCl_4) 3054 (Ar), 2976, 2937 (CH_2, CH_3), 2124 (CC), 1223, 1149, 1105, 1028 (OTf) cm^{-1}; UV−vis (CH_2Cl_2) λ_{max} = 324 nm, $\epsilon = 9.0 \times 10^4$ L cm^{-1} mol^{-1}; ^1H NMR (acetone-d_6) δ 8.65 (d, 8H, $^3J_{HH}$ = 4.7 Hz), 7.70−7.63 (*o*, m, 16H), 7.44−7.37 (*m*, *p*, m, 24H), 6.70 (c, d, 8H, $^3J_{HH}$ = 6.2 Hz), 2.87 (c, bs, 8H), 2.10−2.00 (obscured, 8H), 2.00−1.85 (m, 24H), 1.40−1.27 (m, 36H); $^{13}C\{^1H\}$ NMR (acetone-d_6) δ 134.4 (Pt−P−C*o*), 131.4 (Pt−P−C_{ipso}), 131.8 (Pt−P−C_p), 129.3 (Pt−P−C_m), 149.9 ($C_{\alpha pyr}$), 128.8 ($C_{\beta pyr}$), 140.5 ($C_{ipso pyr}$), 107.7 (t, $^2J_{P-C}$ = 16.9 Hz, CC−Pt_{β}), 122.4 (q, J_{C-F} = 322 Hz, OTf), 24.8 (m, Pt−P−CH_2), 20.1 (bs, CH_2), 16.4 (m, Pd−P−*CH_2*CH_3), 8.4 (bs, Pd−P−CH_2*CH_3*); $^{31}P\{^1H\}$ NMR (acetone-d_6) δ 31.6 (s), −1.9 (s, J_{Pt-P} = 2175 Hz); ^{19}F NMR (acetone-d_6) δ −75. Anal. Calcd for $Pt_2Pd_2C_{110}H_{128}P_8S_4N_4O_{12}F_{12}$: C, 45.48; H, 4.44; N, 1.93; S, 4.41. Found: C, 45.59; H, 4.53; N, 1.91; S, 4.28.

Cyclobis[[*cis*-Pt(dppp)(4-ethynylpyridine)2][*cis*-Pd^{2+}(PEt$_3$)$_2$2$^-$-OSO$_2$CF$_3$]]·2 AgOTf Complex (15). To a solution square **14** (39.4 mg, 0.014 mmol) dissolved in 750 μL of acetone-d_6 in a 7 mm NMR tube at 25 °C was added 2 equiv (7.0 mg, 0.028 mmol) of AgOTf in one portion, and then the reaction mixture was shaken. The solvent was removed under a stream of nitrogen at room temperature followed by solvent removal in vacuo (46.0 mg, 99%): mp 179−182 °C dec; IR (CCl_4) 3059 (Ar), 2966, 2939 (CH_2, CH_3), 2091 (CC), 1257, 1151, 1027 (OTf) cm^{-1}; UV−vis (CH_2Cl_2) λ_{max} = 318 nm, $\epsilon = 8.7 \times 10^4$ L cm^{-1} mol^{-1}; ^1H NMR (acetone-d_6) δ 8.79 (d, 8H, $^3J_{HH}$ = 4.7 Hz), 7.80−7.66 (*o*, m, 16H), 7.49−7.38 (*m*, *p*, m, 24H), 6.82 (d, 8H, $^3J_{HH}$ = 6.0 Hz), 3.03 (bs, 8H), 2.20−2.10 (obscured, 8H), 2.00−1.90 (m, 24H), 1.40−1.27 (m, 36H); $^{13}C\{^1H\}$ NMR (acetone-d_6) δ 134.3 (Pt−P−C*o*), 129.8 (Pt−P−C_{ipso}), 132.4 (Pt−P−C_p), 129.7 (Pt−P−C_m), 150.4 ($C_{\alpha pyr}$), 129.4 ($C_{\beta pyr}$), 137.0 ($C_{ipso pyr}$), 110.1 (m, CC−Pt_{β}), 122.1 (q, J_{C-F} = 320 Hz, OTf), 23.9 (m, Pt−P−CH_2), 19.7 (bs, CH_2), 16.6 (m, Pd−P−*CH_2*CH_3), 8.4 (bs, Pd−P−CH_2*CH_3*); $^{31}P\{^1H\}$ NMR (acetone-d_6) δ 31.8 (s), −4.6 (s, J_{Pt-P} = 2341 Hz); ^{19}F NMR (acetone-d_6) δ −75.

Cyclobis[[*cis*-Pt(dppp)(4-ethynylpyridine)$_2$][*cis*-Pt^{2+}(dppp)2$^-$-OSO$_2$CF$_3$]]·2AgOTf Complex (16). To a solution of square **11** in 750 μL CD_2Cl_2 in a 7 mm NMR tube (32.0 mg, 0.014 mmol) was added 2 equiv (4.8 mg, 0.028 mmol) of AgOTf in one portion at 25 °C, and then the reaction mixture was shaken. The solvent was removed under a stream of nitrogen at room temperature followed by solvent removal in vacuo (36.3 mg, 99%): mp 188−191 °C dec; IR (CCl_4) 3057, 3096 (Ar), 2926 (CH_2), 2081 (CC), 1256, 1156, 1103, 1027 (OTf) cm^{-1}; UV−vis (CH_2Cl_2) λ_{max} = 314 nm, $\epsilon = 8.4 \times 10^4$ L cm^{-1} mol^{-1}; ^1H NMR (CD_2Cl_2) δ 8.26 (d, 8H, $^3J_{HH}$ = 5.1 Hz), 7.70−7.20 (m, 80H), 6.27 (d, 8H, $^3J_{HH}$ = 6.0 Hz), 3.19 (bs, 8H), 2.64 (bs, 8H), 2.12 (m, 8H); $^{13}C\{^1H\}$ NMR (CD_2Cl_2) δ 133.5 (Pt−P−C_o), 129.0−130.0 (Pt−P−C_{ipso}), 132.4 (Pt−P−C_p), 129.6 (Pt−P−C_m), 133.7 (Pt′−P−C_o), 132.8 (Pt′−P−C_p), 129.8 (Pt′−P−C_m), 125.0 (Pt′−P−C_{ipso}), 149.4 ($C_{\alpha pyr}$), 129.3 ($C_{\beta pyr}$), 135.4 ($C_{ipso pyr}$), 125.7−124.6 (obscured, q, CC−Pt_{α}), 121.4 (q, J_{C-F} = 318 Hz, OTf), 26.3 (Pt−P−CH_2), 21.8 (Pt′−P−CH_2), 20.6 (CH_2), 18.2 (CH'_2); $^{31}P\{^1H\}$ NMR (CD_2Cl_2) δ −6.2 (s, J_{Pt-P} = 2355 Hz), −11.1 (s, J_{Pt-P} = 3057 Hz); ^{19}F NMR (CD_2Cl_2) δ −75; FAB LRMS, *m/z* 3799.9 (M − OTf), *m/z* 1824.0 (M − 2OTf).

Acknowledgment. Dedicated to Professor G. J. Karabatsos on the occasion of his 65th birthday. Financial support by the NSF (CHE-9529093, CHE-9002690), University of Utah Institutional Funds Committee and the generous loan of platinum(II) dichloride from Johnson-Matthey are gratefully acknowledged as is the A. von Humboldt Foundation and the hospitality of Professor M. Regitz during the summer of 1996. The authors also thank Professor Robin D. Rogers at the University of Alabama for X-ray structure determination.

Supporting Information Available: Tables of positional parameters and esds, anistropic displacement parameters, and an extended list of bond lengths and bond angles for compound **14** (11 pages). See any current masthead page for ordering and internet access instructions.

JA9635286